iScience

CellPress
OPEN ACCESS

Article

RRM2 promotes liver metastasis of pancreatic cancer by stabilizing YBX1 and activating the TGF-beta pathway

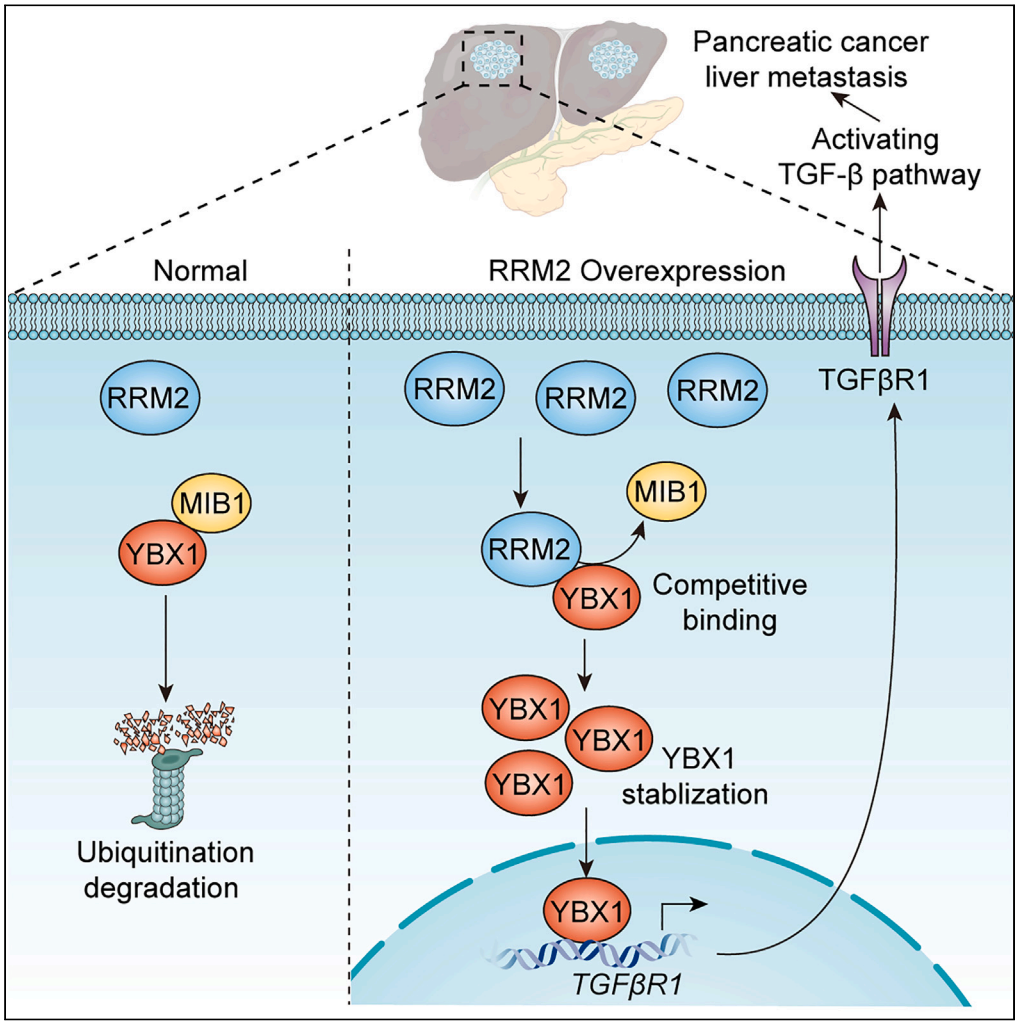

Zhouyuan Du, Qun Zhang, Xingxing Xiang, Wei Li, Qinglin Yang, Haixin Yu, Tao Liu

haixin.y@outlook.com (H.Y.)
uniontao@hust.edu.cn (T.L.)

Highlights

RRM2 is a potential therapeutic target for pancreatic cancer liver metastasis

RRM2 activate the TGF-beta pathway by stabilizing YBX1

RRM2-YBX1-TGFBR1 axis exists in pancreatic cancer that promotes liver metastasis

Du et al., iScience 27, 110864
October 18, 2024
https://doi.org/10.1016/j.isci.2024.110864

iScience

CellPress
OPEN ACCESS

Article

RRM2 promotes liver metastasis of pancreatic cancer by stabilizing YBX1 and activating the TGF-beta pathway

Zhouyuan Du,[1,2] Qun Zhang,[1,2] Xingxing Xiang,[1,2] Wei Li,[1,2] Qinglin Yang,[1,2] Haixin Yu,[1,2,3,*] and Tao Liu[1,2,*]

SUMMARY

Pancreatic cancer is one of the most malignant types of cancer, and despite recent advances in treatment, prognosis remains extremely poor. The most common site of pancreatic cancer metastasis is the liver. Elucidating the molecular mechanisms of pancreatic cancer progression and liver metastasis is essential for improving patients' survival. Ribonucleotide reductase subunit M2 (RRM2) has been linked to many types of cancers and is associated with tumor progression. However, the role of RRM2 in the liver metastasis of pancreatic cancer is still unclear. In this study, RRM2 was found to promote the malignant biological behavior of pancreatic cancer and enhance its liver metastasis. Further studies on the downstream molecular mechanisms of RRM2 revealed that RRM2 stabilizes YBX1, upregulates TGFBR1, and activates the TGF-beta pathway to promote pancreatic cancer progression and liver metastasis. In summary, these results suggest that RRM2 may be an effective therapeutic target for pancreatic cancer liver metastasis.

INTRODUCTION

Pancreatic cancer is a highly heterogeneous disease that accounts for 3% of all malignancies and has a dismal five-year survival rate.[1] Unfortunately, in recent decades, the incidence of pancreatic cancer has been increasing annually. In the past two decades, a significant escalation has been observed in the annual incidence of pancreatic cancer on a global scale, with the number of diagnoses effectively doubling. In 1990, the global count stood at 196,000 cases, which starkly contrasts with the 441,000 cases reported in 2017. This substantial increase can be primarily attributed to the demographic shifts within the global population, coupled with advancements in diagnostic techniques. Notably, these factors have contributed to a pronounced rise in the incidence of pancreatic cancer, particularly within high-income nations. The occurrence of pancreatic cancer is associated with genetic factors, including pathogenic mutations in oncogenes.[2] Despite significant advances in adjuvant therapies that enhance survival, the overall five-year survival rate has barely improved. For patients with resectable pancreatic tumors, the standard therapeutic approach involves adjuvant chemotherapy administered subsequent to surgical resection, typically employing a combination of gemcitabine and capecitabine. The median overall survival (OS) for this patient cohort was recorded at 26 months, with a 5-year survival rate estimated at 30%.[3] The liver is one of the most common sites of metastasis for pancreatic cancer, with approximately 30–40% of patients developing liver metastasis.[4] The median survival time of patients who have liver metastasis of pancreatic cancer remains less than 6 months, regardless of whether they undergo surgical resection or palliative treatment.[5] Therefore, elucidating the mechanisms of pancreatic cancer development and liver metastasis to identify potential therapeutic targets is essential for improving patient outcomes.

Ribonucleotide reductase (RR) consists of two subunits: a large subunit (RRM1) and a small subunit (RRM2 or RRM2B). Dysregulation of RR and abnormal expression of its subunits are implicated in various types of cancers.[6–8] Specifically, RRM2 is overexpressed in several tumors and correlates with tumor progression.[9,10] In pancreatic cancer, RRM2 has been implicated in gemcitabine resistance.[11] However, its role in pancreatic cancer progression and liver metastasis remains unclear.

Previous studies have shown that the TGF-beta signaling pathway plays a crucial role in the liver metastasis of tumors.[12] Y-box binding protein 1 (YBX1) is an oncogene that functions in various tumors[13] and can promote the transcription of TGFBR1.[14] In the present study, we found that RRM2 promotes pancreatic cancer progression and liver metastasis by stabilizing YBX1 and activating the TGF-beta pathway via increased TGFBR1 transcription. These findings suggest that RRM2 is a potential therapeutic target for the treatment of pancreatic cancer liver metastasis.

[1]Department of Digestive Surgical Oncology, Union Hospital, Tongji Medical College, Huazhong University of Science and Technology, Wuhan, China
[2]Cancer Center, Union Hospital, Tongji Medical College, Huazhong University of Science and Technology, Wuhan, China
[3]Lead contact
*Correspondence: haixin.y@outlook.com (H.Y.), uniontao@hust.edu.cn (T.L.)
https://doi.org/10.1016/j.isci.2024.110864

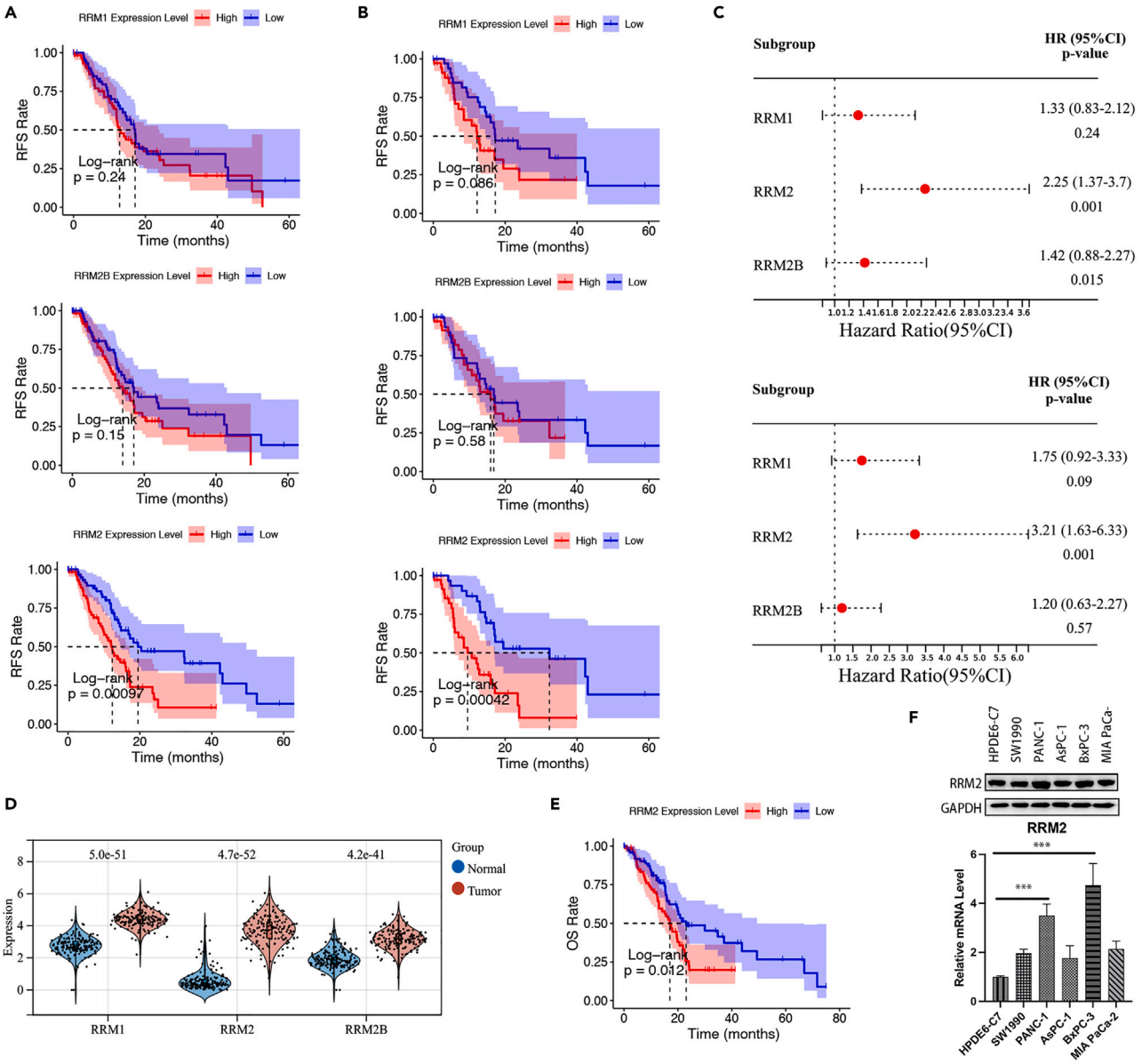

Figure 1. RRM2 overexpression is correlated with poor prognosis and liver metastasis in pancreatic cancer

(A) Disease-free survival of high/low RRM1/RRM2B/RRM2 groups in the TCGA dataset, *p* values as indicated.

(B) Liver metastasis-free survival of high/low RRM1/RRM2B/RRM2 groups in the TCGA dataset, *p* values as indicated.

(C) Forest plot of disease-free survival and liver metastasis-free survival in RRM1/RRM2B/RRM2 groups in the TCGA dataset, HR and 95%CI as indicated.

(D) RRM1/RRM2B/RRM2 gene expression of normal/tumor groups in the TCGA database, *p* values as indicated.

(E) Overall survival of high/low RRM2 groups in the TCGA dataset, *p* values as indicated.

(F) Cells were obtained and used for western blotting analysis and RT-qPCR analysis. The data were exhibited as the mean accompanied by the standard deviation (SD), with three replicates ($n = 3$). The statistical significance of the results was determined using the one-way analysis of variance (ANOVA). ***, $p < 0.001$.

RESULTS

RRM2 overexpression is correlated with poor prognosis and liver metastasis in pancreatic cancer

In this study, we performed Kaplan-Meier survival analysis on the The Cancer Genome Atlas (TCGA) dataset and found that high expression of RR subunits correlated with shorter recurrence-free survival (RFS) and liver metastasis-free survival in pancreatic cancer patients. In particular, RRM2 showed a significant association with shorter RFS and liver metastasis-free survival ($p < 0.001$; Figures 1A and 1B). Furthermore, we conducted a comprehensive analysis of the relationships between RR family protein subunits and tumor RFS and liver

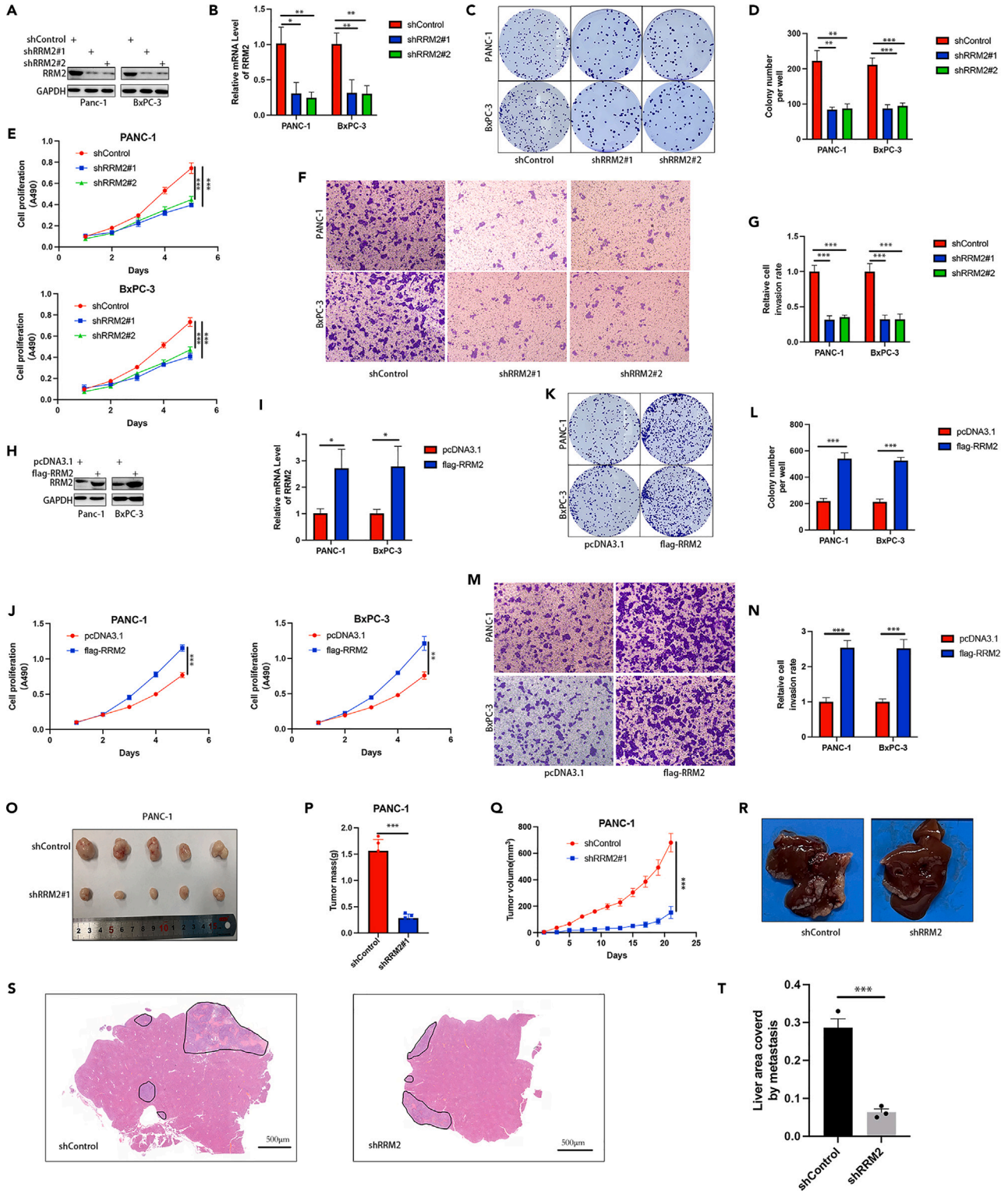

Figure 2. RRM2 promotes pancreatic cancer cell progression and liver metastasis

(A–G) PANC-1 and BxPC-3 cells were infected with the indicated shRNA for 72 h. Cells were collected for western blotting analysis (A), RT-qPCR analysis (B), colony formation assay (C and D), MTS assay (E) and transwell assay (F–G).

For panels B, D, E, and G, data are shown as mean ± SD, with three replicates. Statistical significance was determined by one-way ANOVA. *, $p < 0.05$; **, $p < 0.01$; ***, $p < 0.001$.

Figure 2. *Continued*

(H–N) PANC-1 and BxPC-3 cells were transfected with the indicated plasmid for 48 h. Cells were collected for western blotting analysis (H), RT-qPCR analysis (I), colony formation assay (K and L), MTS assay (J) and transwell assay (M and N).

For panels I, J, L, and N, data are shown as mean ± SD, with three replicates.

Statistical significance was determined by one-way ANOVA. *, $p < 0.05$; **, $p < 0.01$; ***, $p < 0.001$. (O–T) *In vivo* animal experiments. PANC-1 cells were infected with the indicated shRNA for 72 h followed by puromycin selection, then harvested and injected subcutaneously into nude mice to establish a xenograft model (O–Q) and into the spleen to construct a liver metastasis model (R–T).

Tumor images (O), tumor mass (P), tumor growth curve (Q), liver images (R), liver HE-stained sections (S), liver section metastasis area (T). For panels P, Q, and T, data are shown as mean ± SD, with three replicates. Student's t-test was used to determine statistical significance. ***, $p < 0.001$.

metastasis-free survival. RRM2 was found to be the most prognostic factor for poor outcomes (Figure 1C). RRM2 expression was also significantly elevated in tumor tissues compared with normal tissues (Figure 1D). Kaplan-Meier survival analysis of OS revealed that high expression levels of RRM2 were also associated with shorter OS ($p < 0.05$; Figure 1E). Furthermore, comparative analysis revealed an upregulation of RRM2 mRNA in pancreatic cancer cell lines relative to non-malignant pancreatic ductal epithelial cells. This trend was corroborated at the protein level, with elevated RRM2 expression observed in both PANC-1 and BxPC-3 cell lines when juxtaposed with their non-malignant counterparts (Figure 1F). These results indicate that RRM2 may be implicated in pancreatic cancer progression and liver metastasis.

RRM2 promotes pancreatic cancer cell progression and liver metastasis

Next, we examined the oncogenic function of RRM2 in pancreatic cancer by silencing its expression using shRNA in PANC-1 and BxPC-3 pancreatic cancer cells (Figures 2A and 2B). MTS (Tetrazolium inner salt; cell proliferation assay reagent) and colony formation assays showed that RRM2 silencing significantly inhibited cancer cell proliferation (Figures 2C–2E). In addition, the transwell assay revealed that RRM2 knockdown significantly impaired cell invasion (Figures 2F and 2G). In contrast, we found that RRM2 overexpression (Figures 2H–2J) enhanced the proliferation and invasion abilities of PANC-1 and BxPC-3 cells (Figures 2K–2N).

To determine the effect of RRM2 on the *in vivo* growth of pancreatic cancer cells, we subcutaneously injected PANC-1 cells (infected with shControl or shRRM2#1) into nude mice and evaluated tumor growth. We found that RRM2 knockdown significantly reduced tumor growth (Figures 2O–2Q). Moreover, to study the impact of RRM2 knockdown on liver metastases, we constructed a liver metastasis model by injecting PANC-1 cells transfected with shControl or shRRM2#1 into the spleen. RRM2 silencing was found to inhibit the ability of pancreatic cancer cells to develop liver metastasis (Figures 2R–2T). The aforementioned *in vivo* and *in vitro* experiments demonstrated that RRM2 plays an important role in pancreatic cancer progression and liver metastasis.

RRM2 activates TGFBR1 in pancreatic cancer

To elucidate the mechanism by which RRM2 regulates the progression and liver metastasis of pancreatic cancer, we predicted that RRM2 was significantly associated with EMT, based on data mining single-cell datasets from lung adenocarcinoma (EXP0066) and glioma (EXP0060) (Figures 3A–3D). The TGF-beta pathway is significantly associated with tumor EMT (epithelial-mesenchymal transition). we analyzed an RNA-seq dataset (GSE117924), finding that RRM2 knockdown reduced the expression of TGFBR1 and TGFBR2 in the TGF-beta pathway (Figures 3E and 3F). Furthermore, our analysis of RNA-sequencing data from PANC-1 cells revealed that RRM2 knockdown significantly attenuated the expression levels of TGFBR1 (Figures 3G and 3H). Further experiments showed that RRM2 knockdown reduced the protein level of TGFBR1 (Figure 3I), while RRM2 overexpression increased TGFBR1 protein abundance (Figure 3K). Meanwhile, in a pancreatic cancer tissue microarray ($n = 45$, Spearman $r = 0.5956$, $p < 0.001$), RRM2 protein levels were positively correlated with TGFBR1 protein levels (Figures 3K and 3L). In addition, western blot revealed that RRM2 knockdown inhibits the expression of *p*-SMAD2/3 through TGFBR1. (Figures S1A–S1D). Therefore, the previous results indicated that RRM2 may activate TGF-beta pathway via TGFBR1 in pancreatic cancer.

RRM2 binds to YBX1 to activate TGFBR1

To explore the mechanism by which RRM2 activates TGFBR1 in pancreatic cancer cells, we identified potential binding partners of RRM2 through published mass spectrometry results (Figure 4A). In this mass spectrometry analysis, we found that YBX1 was one of the important binding partners of RRM2. According to the literature, YBX1 can promote transcription and activate TGFBR1.[14] Therefore, we hypothesized that RRM2 activates TGFBR1 through YBX1. Co-immunoprecipitation (coIP) and immunofluorescence co-localization confirmed that RRM2 interacts with YBX1 in pancreatic cancer cells (PANC-1 and BxPC-3) (Figures 4B and 4C). Further, in the pancreatic cancer tissue microarray ($n = 45$, Spearman $r = 0.6345$, $p < 0.001$), RRM2 expression level was positively correlated with YBX1 expression level (Figures 4D and 4E). These results indicate that RRM2 can bind to and regulate the protein level of YBX1 in pancreatic cancer. To further elucidate the mechanism by which YBX1 regulates TGFBR1, we analyzed a publicly available YBX1 ChIP-seq dataset and found that there was a significant YBX1 binding peak in the gene promoter region of TGFBR1 (Figure 4F), which was further confirmed by chromatin immunoprecipitation quantitative real-time PCR (ChIP-qPCR) analysis in pancreatic cancer cells PANC-1 and BxPC-3 (Figure 4G). As expected, shRNA knockdown of YBX1 resulted in significant decrease of TGFBR1 (Figures 4H and 4I). These results indicate that YBX1 activates TGFBR1 expression in pancreatic cancer by enhancing its transcription.

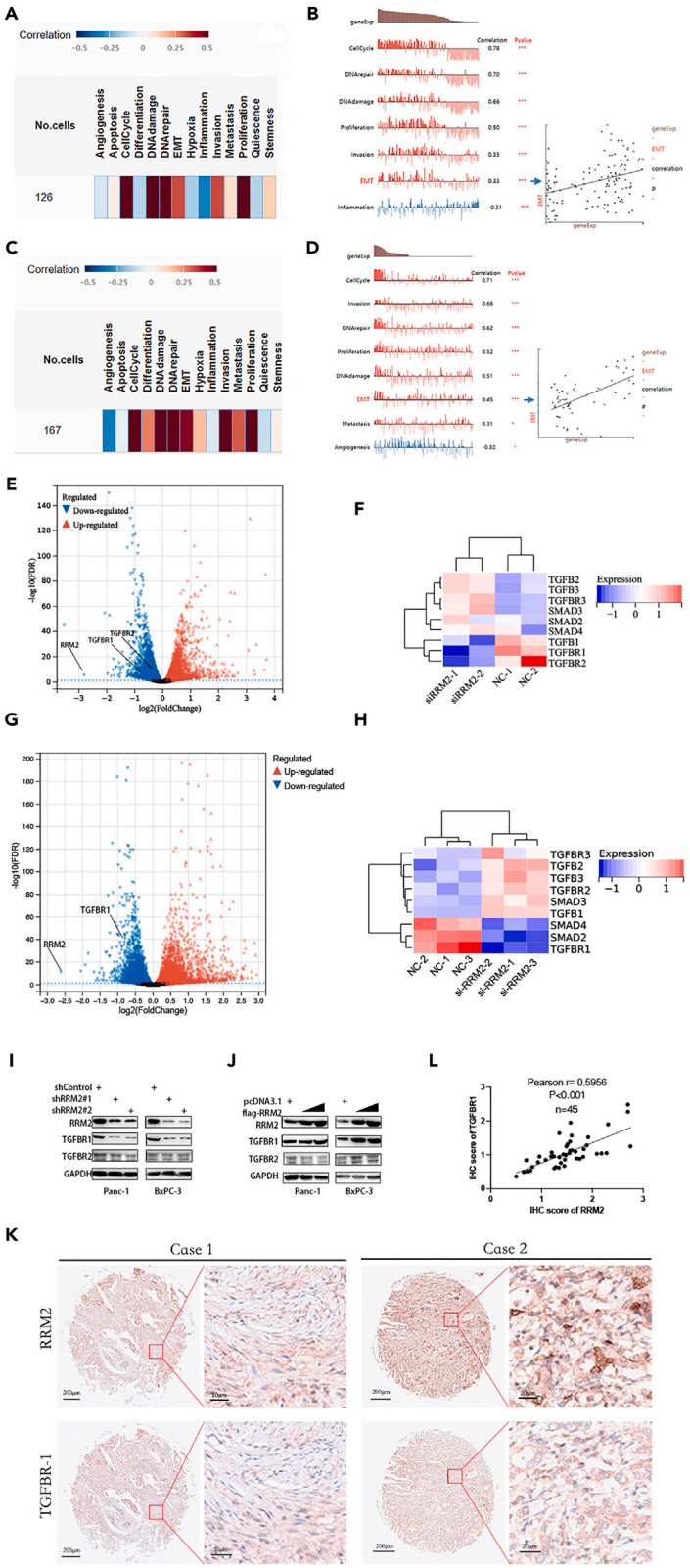
A
Correlation
No.cells
126
Angiogenesis
Apoptosis
CellCycle
Differentiation
DNAdamage
DNArepair
EMT
Hypoxia
Inflammation
Invasion
Metastasis
Proliferation
Quiescence
Stemness
B
C
No.cells
167
D
E
Regulated
Down-regulated
Up-regulated
-log10(FDR)
log2(FoldChange)
RRM2
TGFBR1
TGFBR2
F
Expression
TGFB2
TGFB3
TGFBR3
SMAD3
SMAD2
SMAD4
TGFB1
TGFBR1
TGFBR2
siRRM2-1
siRRM2-2
NC-1
NC-2
G
H
NC-2
NC-1
NC-3
si-RRM2-2
si-RRM2-1
si-RRM2-3
I
shControl
shRRM2#1
shRRM2#2
GAPDH
Panc-1
BxPC-3
J
pcDNA3.1
flag-RRM2
L
Pearson r= 0.5956
P<0.001
n=45
IHC score of TGFBR1
IHC score of RRM2
K
Case 1
Case 2
TGFBR-1

Figure 3. RRM2 activates TGFBR1 in pancreatic cancer

(A–D) Single-cell data mining in the CancerSEA database. Results from lung adenocarcinoma single-cell dataset EXP0066 (A and B) and glioma single-cell dataset EXP0060 (C and D). In panels B and D, the correlation and *p* value are as indicated, *, $p < 0.05$; ***, $p < 0.001$.

(E and F) GEO database analysis of dataset GSE117924; volcano plot (E) and heatmap (F) analysis of the expression of TGF-beta pathway target genes after silencing RRM2.

(G and H) PANC-1 cells were infected for 72 h, and cells were collected for RNA-seq analysis; volcano plot (G) and heatmap (H) analysis of the expression of TGF-beta pathway target genes after silencing RRM2.

(I) PANC-1 and BxPC-3 cells were infected with the indicated shRNA for 72 h, and cells were collected for western blot analysis.

(J) PANC-1 and BxPC-3 cells were infected with the indicated plasmid for 48 h, and cells were collected for western blot analysis.

(K and L) A pancreatic cancer tissue microarray was stained for RRM2 and TGFBR1 ($n = 45$). Panel K shows the IHC images, scale as indicated. Panel L shows the correlation of the expression of the two proteins, using Pearson's correlation to determine statistical significance, *p* value as shown.

RRM2 regulates tumor progression and liver metastasis through YBX1 in pancreatic cancer

We next sought to elucidate how the interaction between RRM2 and YBX1 influences pancreatic cancer progression and liver metastasis. RRM2 knockdown resulted in decreased TGFBR1 expression, an effect that was enhanced by YBX1 knockdown (Figure 5A). On the other hand, overexpression of RRM2 resulted in increased TGFBR1 expression, which was inhibited by knocking down YBX1 (Figure 5B). We further examined the effects of RRM2 and YBX1 silencing on pancreatic cancer cell proliferation and invasion *in vitro*. Colony formation assay and MTS assay showed that RRM2 and YBX1 silencing significantly inhibited pancreatic cancer cell proliferation *in vitro* (Figures 5C–5E). Similarly, transwell assay showed that RRM2 and YBX1 silencing impaired the invasion ability of pancreatic cancer cells (Figures 5F and 5G). To determine whether these effects are preserved *in vivo*, we subcutaneously injected PANC-1 cells (shControl; shRRM2; shYBX1; shRRM2+shYBX1) into nude mice and evaluated tumor growth (Figures 5H–5J). To model liver metastasis, we also injected the previous cells into the spleen (Figures 5K–5M). We found that the combined silencing of RRM2 and YBX1 further inhibited pancreatic cancer proliferation and liver metastasis *in vivo*, compared to knockdown of either molecule alone. These results indicate that RRM2 regulates TGFBR1 through YBX1, thereby affecting pancreatic cancer progression and liver metastasis.

RRM2 competes with MIB1 to stabilize YBX1 in pancreatic cancer cells

The previous results showed that RRM2 silencing reduced the protein level of YBX1 in pancreatic cancer, and RRM2 overexpression increased YBX1 protein levels (Figures 5A and 5B). To investigate YBX1 stability, cells were treated with the 26S proteasome inhibitor MG132, which was found to attenuate the decrease in YBX1 induced by RRM2 silencing (Figure 6A). In addition, RRM2 knockdown shortened the half-life of YBX1 and enhanced its ubiquitination (Figures 6B and 6D). Conversely, RRM2 overexpression prolonged the half-life of YBX1 and reduced the ubiquitination level of YBX1 (Figures 6C and 6E). We next sought to elucidate the mechanisms of YBX1 ubiquitination. Predicted E3 ligases were compared from different databases and common hits were identified (Figure 6F). These were combined with possible E3 ligases that ubiquitinate YBX1 as reported in Ubibrowser (Figure 6G). Thus, we identified 5 possible E3 ligases that ubiquitinate YBX1, and performed shRNA silencing of each one individually. The results showed that MIB1 knockdown in pancreatic cancer cells produced the most significant increase in YBX1 protein levels (Figure 6H). coIP confirmed that MIB1 interacted with YBX1 in PANC-1 and BxPC-3 pancreatic cancer cells (Figure 6I). Silencing MIB1 increased the protein level of YBX1 in pancreatic cancer cells but did not increase the mRNA level (Figure 6J). Knocking down MIB1 prolonged the half-life of YBX1 in PANC-1 cells (Figure 6K), and reduced the ubiquitination level (Figure 6L), implying that YBX1 is a substrate of MIB1 in PANC-1 cells. Moreover, RRM2 exhibited competitive binding to YBX1 with MIB1 (Figures 6M–6O). These results indicate that RRM2 binds and stabilizes YBX1 by competing with MIB1 in pancreatic cancer.

DISCUSSION

Pancreatic cancer is a highly aggressive malignancy with extremely poor prognosis. Due to the lack of specific early symptoms, it is incredibly difficult to diagnose pancreatic cancer at an early stage, and, consequently, most patients present with advanced or metastatic disease at the time of diagnosis.[15,16] The liver is one of the most frequent sites of metastasis of pancreatic cancer. Patients with metastatic pancreatic cancer have very poor outcomes, and surgery is rarely curative. Current systemic treatments for metastatic pancreatic cancer include first-line regimens such as FOLFIRINOX and gemcitabine + Nab-Paclitaxel, but only a minority of patients can benefit from targeted therapies.[16,17] For patients with liver metastasis from pancreatic cancer, survival is typically less than 6 months.[4] Hence, there is a great unmet need for more effective treatment strategies and targets. Our present study revealed that RRM2 is associated with the progression and liver metastasis of pancreatic cancer and may represent a potential therapeutic target in the future. Moreover, we elucidated underlying mechanisms to demonstrate that RRM2 acts through YBX1 and the TGF-beta pathway to influence pancreatic cancer progression, including in the context of liver metastasis. Our investigation suggests that RRM2 could serve as a promising diagnostic biomarker, and its targeted modulation may exert a significant influence on the therapeutic landscape of pancreatic cancer.

RRM2 is a subunit of ribonucleotide reductase, which catalyzes the synthesis of deoxyribonucleotides for mitochondrial and nuclear DNA repair and replication.[18] RRM2 is frequently overexpressed in various malignancies, such as liver cancer, kidney cancer, prostate cancer, and others.[9,18,19] In pancreatic cancer, RRM2 inhibition enhances chemosensitivity to gemcitabine, a first-line chemotherapeutic agent for pancreatic cancer.[20,21] In this study, we explored the role of RRM2 in pancreatic cancer progression and liver metastasis. We demonstrated that RRM2 overexpression correlated with poor survival and increased liver metastasis in pancreatic cancer patients, and that RRM2 knockdown impaired

A

Accession	Gene	Mw(kDa)	RRM2-IgG	RRM2-IP	log2(RRM2-IP/RRM2-IgG)	Diff Sig
P04083	ANXA1	38.71	19.2299	29.2485	10.019	++
P31350	RRM2	44.88	21.0895	31.0046	9.9151	++
P09874	PARP1	113.1	22.8697	31.4702	8.6005	++
H3BT71	RBMX	32.2	18.2314	25.7414	7.51	++
		.....				
P67809	YBX1	35.92	18.8599	23.7652	4.9053	++

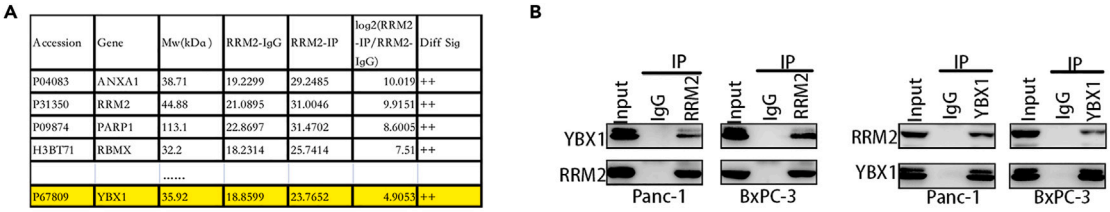

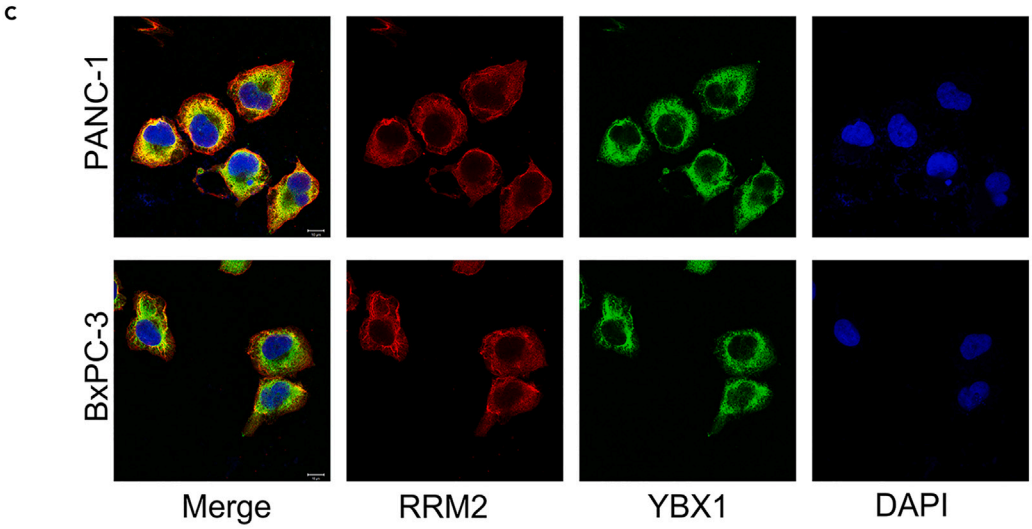

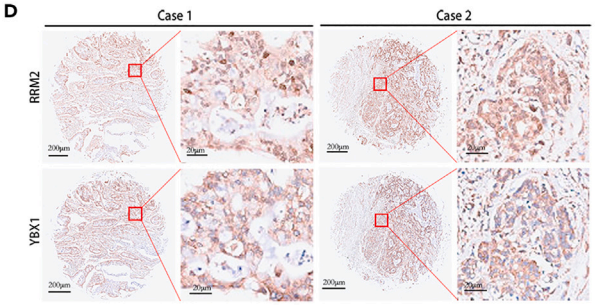

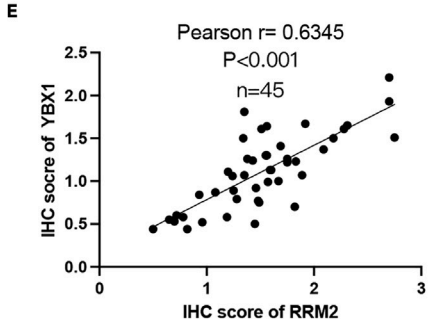

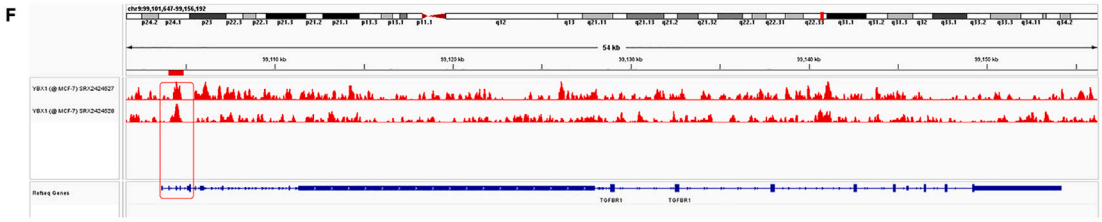

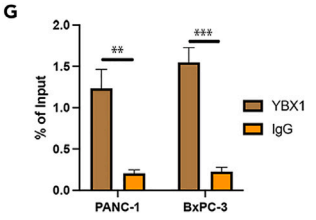

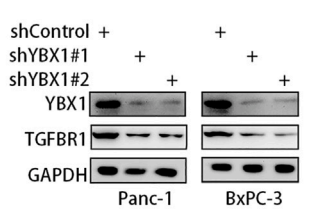

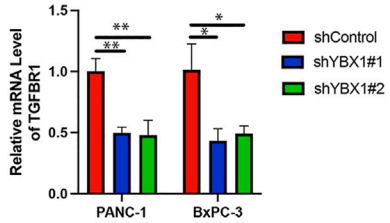

Figure 4. RRM2 binds to YBX1 to activate TGFBR1

(A) Mass spectrometry analysis of RRM2 binding partners.

(B) Western blotting analysis of whole cell lysate (WCL) from PANC-1 and BxPC03 cells.

(C) Immunofluorescence co-localization of RRM2 and YBX1 in PANC-1 and BxPC-3 cells.

(D and E) Tissue microarray of pancreatic cancer samples stained for RRM2 and YBX1 (n = 45). Panel D shows IHC images, scale as shown. Panel E shows the correlation of the two proteins; Pearson's correlation was used to determine statistical significance, p values as shown.

(F) ChIP Atlas was used to visualize the binding of YBX1 at the TGFBR1 gene locus.

(G) ChIP-qPCR of PANC-1 and BxPC-3 cells. All data show mean ± SD of 3 replicates, statistical significance determined by Student's t test. **, $p < 0.01$; ***, $p < 0.001$.

(H and I) PANC-1 and BxPC-3 cells were infected with the indicated shRNA for 72 h, and cells were harvested for western blotting analysis (H) and RT-qPCR (I). The data were exhibited as the mean accompanied by the standard deviation (SD), with three replicates (n = 3). The statistical significance of the results was determined using the one-way analysis of variance (ANOVA).*, $p < 0.05$; **, $p < 0.01$.

the proliferation and invasion of pancreatic cancer cells and inhibited liver metastasis *in vivo*. However, the underlying mechanism of RRM2 regulation remained elusive. It was known that RRM2 overexpression activated the TGF-beta signaling pathway,[22] which is implicated in tumor liver metastasis.[12] We also found that RRM2 upregulated the expression of TGFBR1, a receptor for TGF-beta, based on bioinformatics analysis of public datasets. Therefore, we hypothesized that RRM2 may promote pancreatic cancer progression and liver metastasis through modulating the TGF-beta pathway. We then investigated the mechanisms by which RRM2 regulates the TGF-beta pathway, and found mass spectrometry data in the literature indicating an interaction between RRM2 and YBX1.[9] YBX1 is a transcription factor that exerts oncogenic functions in various cancers.[14,23,24] For example, YBX1 antibody enhances CBX3 transcription to suppress SMURF2-mediated smoking-induced pancreatic cancer progression.[23] In breast cancer, YBX1 elevates CTPS1 expression, facilitating cell proliferation and invasion.[24] Previous studies have shown that in non-small cell lung cancer, YBX1 can activate TGFBR1 transcription.[14] This is consistent with our current results, as we discovered that YBX1 could activate TGFBR1 transcription, and RRM2 could bind to YBX1 and stabilize its protein level. Further investigations revealed that RRM2 interacted with YBX1 in pancreatic cancer by competing with MIB1, increasing its stability. Hence, our results identified a RRM2-YBX1-TGFBR1 axis that exists in pancreatic cancer and regulates pancreatic cancer proliferation, invasion, and liver metastasis.

The liver is one of the most frequent metastatic sites of pancreatic cancer. Numerous studies have investigated the mechanism of pancreatic cancer liver metastasis. Substances secreted by granulocytes and metastasis-associated macrophages (MAMs) have been shown to induce liver fibrosis and play a vital role in pancreatic cancer liver metastasis.[25] Furthermore, the transcription factor GATA2 mediates Notch3 transcriptional activation and promotes pancreatic cancer liver metastasis.[26] Additionally, type I transmembrane glycosylated protein MUC16 has been shown to modulate NRP2 and induce PDAC(pancreatic ductal adenocarcinoma) metastasis.[27] However, there are currently no effective drugs that target these pathways to improve patient survival. According to the extant literature, RRM2 and YBX1 have been implicated in the promotion of pancreatic cancer progression, thereby emerging as potential therapeutic targets. Our study delineates the interaction between RRM2 and YBX1, which synergistically facilitates pancreatic cancer progression and liver metastasis. Moreover, we propose that a combinatorial therapeutic strategy targeting pivotal nodes within this signaling cascade may offer a promising avenue for improving the clinical prognosis of pancreatic cancer patients. Our results provide further insight into the mechanisms by which pancreatic cancer metastasizes to the liver, thus widening the scope of potential therapeutic targets.

In conclusion, our results demonstrate that high expression of RRM2 promotes pancreatic cancer liver metastasis and likely contributes to the poor prognosis of pancreatic cancer patients. An RRM2-YBX1-TGFBR1 axis exists in pancreatic cancer that plays a crucial role in pancreatic cancer liver metastasis. Our study identifies potential therapeutic targets for the treatment of pancreatic cancer liver metastasis.

Limitations of the study

Although our study confirmed the role of RRM2 in promoting pancreatic cancer liver metastasis and its molecular mechanism through *in vivo* and *in vitro* studies, we did not further verify the molecular mechanism using transgenic mice with spontaneously oncogenic pancreatic cancer. In addition, in order to further study the clinical application of this molecular mechanism, it is necessary to further study combined with the current comprehensive treatment of pancreatic cancer.

RESOURCE AVAILABILITY

Lead contact

Further information and requests for resources and reagents should be directed to and will be fulfilled by the lead contact, Dr. Du Zhouyuan (394232374@qq.com).

Materials availability

This study did not generate new unique reagents.

Data and code availability

- RNA-sequencing data that support the findings of this study have been deposited into the Gene Expression Omnibus (GEO) (https://www.ncbi.nlm.nih.gov/geo/query/acc.cgi?acc=GSE274806). All data presented in this study will be shared upon reasonable request by the lead contact, Dr. Du Zhouyuan (394232374@qq.com).

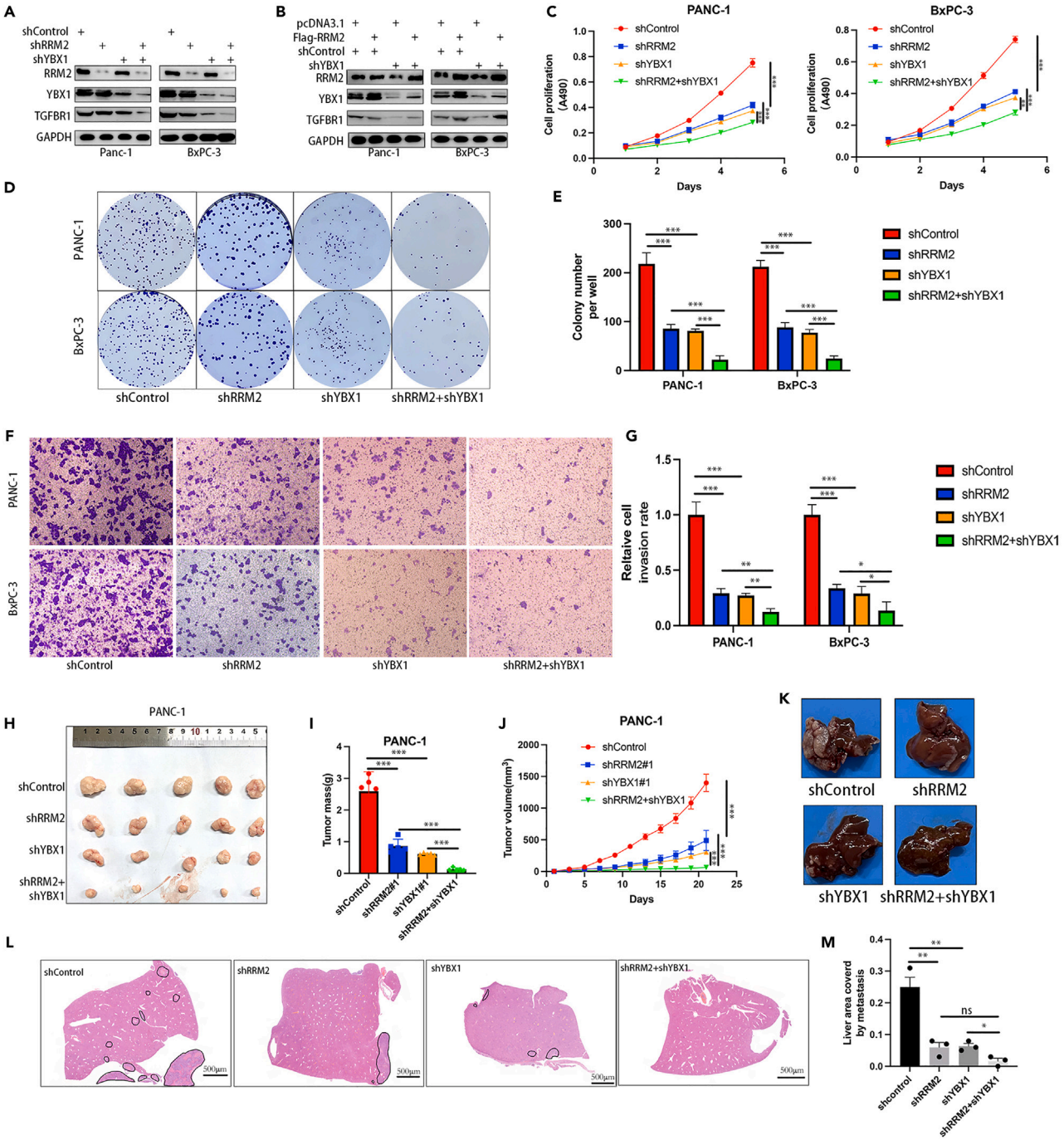

Figure 5. RRM2 regulates tumor progression and liver metastasis through YBX1 in pancreatic cancer

(A) PANC-1 and BxPC-3 cells were infected with the indicated shRNA for 72 h. Cells were harvested for western blot analysis.

(B) PANC-1 and BxPC-3 cells were transfected with the indicated shRNA and plasmid for 48 h. Cells were harvested for western blot analysis.

(C–G) PANC-1 and BxPC-3 cells were infected with the indicated shRNA for 72 h, then used for MTS and colony formation assays (D and E) and transwell assay (F and G). For panels C, E, and G, data are shown as mean ± SD, with three replicates. Statistical significance was determined by one-way ANOVA. *, $p < 0.05$; **, $p < 0.01$; ***, $p < 0.001$.

(H–M) *In vivo* animal experiments. PANC-1 cells were infected with the indicated shRNA for 72 h, and, after puromycin selection, cells were harvested and injected subcutaneously into nude mice for the xenograft experiment (H–J) and into the spleen to establish the liver metastasis model (K–M). Tumor images (H), tumor mass (I), tumor growth curve (J), liver images (K), liver HE-stained sections (L), and liver section metastasis area (M). In panels I, J, M, data are shown as mean ± SD, with three replicates. Student's t-test was used to determine the statistical significance. *, $p < 0.05$; **, $p < 0.01$; ***, $p < 0.001$.

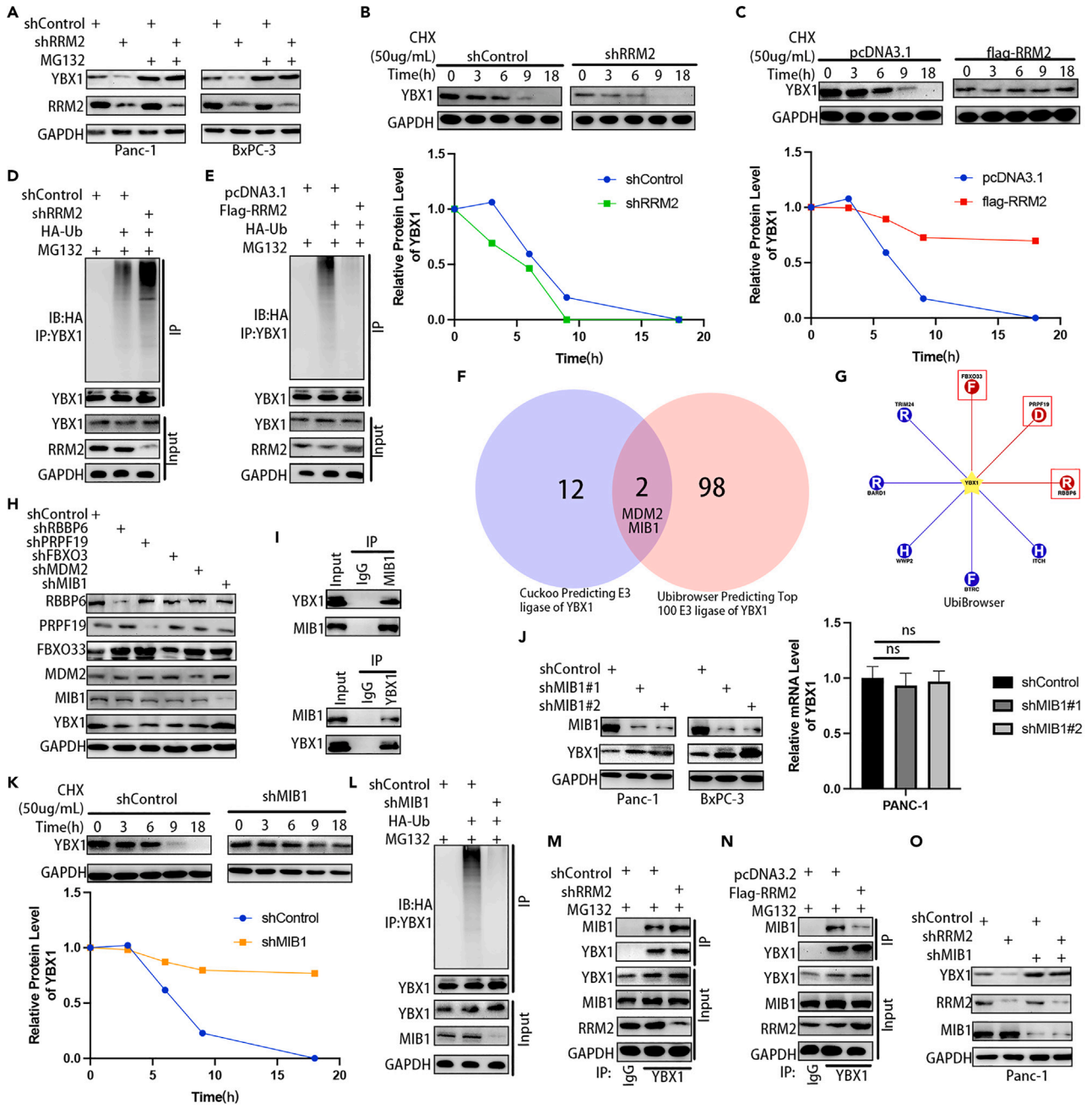

Figure 6. RRM2 competes with MIB1 to stabilize YBX1 in pancreatic cancer cells

(A) PANC-1 cells were infected with the indicated shRNA for 72 h. After treatment with MG132 or vehicle, cells were harvested for western blot analysis.

(B) PANC-1 cells were infected with the indicated shRNA for 72 h, then treated with cycloheximide (CHX) and harvested at different time points for western blot analysis, YBX1 protein quantified using ImageJ.

(C) PANC-1 cells were transfected with the indicated plasmid. After 48 h, cells were treated with CHX and harvested at different time points for western blot analysis, YBX1 protein quantified using ImageJ.

(D) PANC-1 cells were infected with the indicated shRNA for 72 h, then treated with MG132 for 8 h and harvested for western blot analysis.

(E) PANC-1 cells were transfected with the indicated plasmid for 48 h, then treated with MG132 for 8 h and harvested for western blot analysis.

(F) Venn diagram showing intersection of potential E3 ligases that ubiquitinate YBX1.

(G) Possible E3 ligases of YBX1 reported in Ubibrowser.

(H) PANC-1 cells were infected with the indicated shRNA for 72 h, then harvested for western blot analysis.

(I) Western blot analysis of WCL from PANC-1 cells.

Figure 6. *Continued*

(J) PANC-1 and BxPC03 cells were transfected with the indicated plasmid for 72 h, then cells were harvested for western blot analysis and RT-qPCR analysis. Data are shown as mean ± SD, with three replicates. Statistical significance was determined by one-way ANOVA. ns, not significant.

(K) PANC-1 cells were infected with the indicated shRNA for 72 h, then treated with cycloheximide (CHX) and harvested at different time points for western blot analysis, YBX1 protein quantified using ImageJ.

(L) PANC-1 cells were infected with the indicated shRNA for 72 h, then treated with MG132 for 8 h and harvested for western blot analysis.

(M) PANC-1 cells were infected with the indicated shRNA for 72 h, then treated with MG132 for 8 h and harvested for western blot analysis.

(N) Cells were transfected with the indicated plasmid for 48 h, then treated with MG132 for 8 h and harvested for western blot analysis.

(O) PANC-1 cells were transfected with the indicated plasmid and WCL was harvested for western blot analysis.

- This paper does not report any original code.
- Additional information required to reanalyze the data reported in this paper is available from the lead contact upon request.

ACKNOWLEDGMENTS

This work was supported by the Chinese National Natural Science Foundation of China grant no. 81572436 (Tao Liu).

AUTHOR CONTRIBUTIONS

Conceptualization, Z.D. and H.Y.; methodology, Z.D.; software, H.Y.; validation, Z.D., Q.Z.; formal analysis, Z.D.; investigation, Q.Y. and Q.Z.; resources, X.X. and W.L.; data curation, Z.D.; writing—original draft preparation, Z.D.; writing—review and editing, H.Y. and T.L.; visualization, H.Y.; supervision, T.L.; project administration, T.L.; funding acquisition, T.L. All authors have read and agreed to the published version of the manuscript.

DECLARATION OF INTERESTS

The authors declare no competing interests.

STAR★METHODS

Detailed methods are provided in the online version of this paper and include the following:

- KEY RESOURCES TABLE
- EXPERIMENTAL MODEL AND STUDY PARTICIPANT DETAILS
  - Cell lines
  - Animal studies
- METHOD DETAILS
  - Cell transfection
  - Co-immunoprecipitation and immunoblotting
  - RT-qPCR and ChIP-qPCR
  - *In vitro* cell growth assay
  - *In vitro* invasion assay
  - *In vivo* tumor growth assay and liver metastasis assay
  - Tissue microarray and immunohistochemistry (IHC)
  - Immunofluorescence co-localization
  - Bioinformatics analysis
- QUANTIFICATION AND STATISTICAL ANALYSIS

SUPPLEMENTAL INFORMATION

Supplemental information can be found online at https://doi.org/10.1016/j.isci.2024.110864.

Received: March 18, 2024
Revised: July 11, 2024
Accepted: August 29, 2024
Published: August 31, 2024

REFERENCES

1. Siegel, R.L., Miller, K.D., Wagle, N.S., and Jemal, A. (2023). Cancer statistics, 2023. CA A Cancer J. Clin. *73*, 17–48. https://doi.org/10.3322/caac.21763.
2. Klein, A.P. (2021). Pancreatic cancer epidemiology: understanding the role of lifestyle and inherited risk factors. Nat. Rev. Gastroenterol. Hepatol. *18*, 493–502. https://doi.org/10.1038/s41575-021-00457-x.
3. Neoptolemos, J.P., Kleeff, J., Michl, P., Costello, E., Greenhalf, W., and Palmer, D.H. (2018). Therapeutic developments in pancreatic cancer: current and future perspectives. Nat. Rev. Gastroenterol. Hepatol. *15*, 333–348. https://doi.org/10.1038/s41575-018-0005-x.
4. Tsilimigras, D.I., Brodt, P., Clavien, P.A., Muschel, R.J., D'Angelica, M.I., Endo, I., Parks, R.W., Doyle, M., de Santibañes, E., and Pawlik, T.M. (2021). Liver metastases. Nat. Rev. Dis. Prim. *7*, 27. https://doi.org/10.1038/s41572-021-00261-6.
5. Ouyang, H., Wang, P., Meng, Z., Chen, Z., Yu, E., Jin, H., Chang, D.Z., Liao, Z., Cohen, L., and Liu, L. (2011). Multimodality treatment of pancreatic cancer with liver metastases using chemotherapy, radiation therapy, and/or Chinese herbal medicine. Pancreas *40*, 120–125. https://doi.org/10.1097/MPA.0b013e3181e6e398.
6. Jordheim, L.P., Sève, P., Trédan, O., and Dumontet, C. (2011). The ribonucleotide reductase large subunit (RRM1) as a predictive factor in patients with cancer. Lancet Oncol. *12*, 693–702. https://doi.org/10.1016/S1470-2045(10)70244-8.

7. Yin, X., Jiang, K., Zhou, Z., Yu, H., Yan, D., He, X., and Yan, S. (2023). Prognostic and Immunological Potential of Ribonucleotide Reductase Subunits in Liver Cancer. Oxid. Med. Cell. Longev. *2023*, 3878796. https://doi.org/10.1155/2023/3878796.
8. Iqbal, W., Demidova, E.V., Serrao, S., ValizadehAslani, T., Rosen, G., and Arora, S. (2021). RRM2B Is Frequently Amplified Across Multiple Tumor Types: Implications for DNA Repair, Cellular Survival, and Cancer Therapy. Front. Genet. *12*, 628758. https://doi.org/10.3389/fgene.2021.628758.
9. Xiong, W., Zhang, B., Yu, H., Zhu, L., Yi, L., and Jin, X. (2021). RRM2 Regulates Sensitivity to Sunitinib and PD-1 Blockade in Renal Cancer by Stabilizing ANXA1 and Activating the AKT Pathway. Adv. Sci. *8*, e2100881. https://doi.org/10.1002/advs.202100881.
10. Jin, C.Y., Du, L., Nuerlan, A.H., Wang, X.L., Yang, Y.W., and Guo, R. (2020). High expression of RRM2 as an independent predictive factor of poor prognosis in patients with lung adenocarcinoma. Aging (Albany NY) *13*, 3518–3535. https://doi.org/10.18632/aging.202292.
11. Lu, H., Lu, S., Yang, D., Zhang, L., Ye, J., Li, M., and Hu, W. (2019). MiR-20a-5p regulates gemcitabine chemosensitivity by targeting RRM2 in pancreatic cancer cells and serves as a predictor for gemcitabine-based chemotherapy. Biosci. Rep. *39*, BSR20181374. https://doi.org/10.1042/BSR20181374.
12. Marvin, D.L., Heijboer, R., Ten Dijke, P., and Ritsma, L. (2020). TGF-beta signaling in liver metastasis. Clin. Transl. Med. *10*, e160. https://doi.org/10.1002/ctm2.160.
13. Cui, Q., Wang, C., Liu, S., Du, R., Tian, S., Chen, R., Geng, H., Subramanian, S., Niu, Y., Wang, Y., and Yue, D. (2021). YBX1 knockdown induces renal cell carcinoma cell apoptosis via Kindlin-2. Cell Cycle *20*, 2413–2427. https://doi.org/10.1080/15384101.2021.1985771.
14. Yin, H., Chen, L., Piao, S., Wang, Y., Li, Z., Lin, Y., Tang, X., Zhang, H., Zhang, H., and Wang, X. (2023). M6A RNA methylation-mediated RMRP stability renders proliferation and progression of non-small cell lung cancer through regulating TGFBR1/SMAD2/SMAD3 pathway. Cell Death Differ. *30*, 605–617. https://doi.org/10.1038/s41418-021-00888-8.
15. Zhu, H., Li, T., Du, Y., and Li, M. (2018). Pancreatic cancer: challenges and opportunities. BMC Med. *16*, 214. https://doi.org/10.1186/s12916-018-1215-3.
16. De Dosso, S., Siebenhüner, A.R., Winder, T., Meisel, A., Fritsch, R., Astaras, C., Szturz, P., and Borner, M. (2021). Treatment landscape of metastatic pancreatic cancer. Cancer Treat Rev. *96*, 102180. https://doi.org/10.1016/j.ctrv.2021.102180.
17. Ettrich, T.J., and Seufferlein, T. (2021). Systemic Therapy for Metastatic Pancreatic Cancer. Curr. Treat. Options Oncol. *22*, 106. https://doi.org/10.1007/s11864-021-00895-4.
18. Mazzu, Y.Z., Armenia, J., Chakraborty, G., Yoshikawa, Y., Coggins, S.A., Nandakumar, S., Gerke, T.A., Pomerantz, M.M., Qiu, X., Zhao, H., et al. (2019). A Novel Mechanism Driving Poor-Prognosis Prostate Cancer: Overexpression of the DNA Repair Gene, Ribonucleotide Reductase Small Subunit M2 (RRM2). Clin. Cancer Res. *25*, 4480–4492. https://doi.org/10.1158/1078-0432.CCR-18-4046.
19. Yang, Y., Lin, J., Guo, S., Xue, X., Wang, Y., Qiu, S., Cui, J., Ma, L., Zhang, X., and Wang, J. (2020). RRM2 protects against ferroptosis and is a tumor biomarker for liver cancer. Cancer Cell Int. *20*, 587. https://doi.org/10.1186/s12935-020-01689-8.
20. Li, W., Chen, Q., Gao, W., and Zeng, H. (2022). ARID1A promotes chemosensitivity to gemcitabine in pancreatic cancer through epigenetic silencing of RRM2. Pharmazie *77*, 224–229. https://doi.org/10.1691/ph.2022.1881.
21. Liu, Q., Song, C., Li, J., Liu, M., Fu, L., Jiang, J., Zeng, Z., and Zhu, H. (2022). E2F2 enhances the chemoresistance of pancreatic cancer to gemcitabine by regulating the cell cycle and upregulating the expression of RRM2. Med. Oncol. *39*, 124. https://doi.org/10.1007/s12032-022-01715-x.
22. Liu, X., Wang, J., Chen, M., Liu, S., Yu, X., and Wen, F. (2019). Combining data from TCGA and GEO databases and reverse transcription quantitative PCR validation to identify gene prognostic markers in lung cancer. OncoTargets Ther. *12*, 709–720. https://doi.org/10.2147/OTT.S183944.
23. Zhang, H., Yu, H., Ren, D., Sun, Y., Guo, F., Cai, H., Zhou, C., Zhou, Y., Jin, X., and Wu, H. (2022). CBX3 Regulated By YBX1 Promotes Smoking-induced Pancreatic Cancer Progression via Inhibiting SMURF2 Expression. Int. J. Biol. Sci. *18*, 3484–3497. https://doi.org/10.7150/ijbs.68995.
24. Lin, Y., Zhang, J., Li, Y., Guo, W., Chen, L., Chen, M., Chen, X., Zhang, W., Jin, X., Jiang, M., et al. (2022). CTPS1 promotes malignant progression of triple-negative breast cancer with transcriptional activation by YBX1. J. Transl. Med. *20*, 17. https://doi.org/10.1186/s12967-021-03206-5.
25. Nielsen, S.R., Quaranta, V., Linford, A., Emeagi, P., Rainer, C., Santos, A., Ireland, L., Sakai, T., Sakai, K., Kim, Y.S., et al. (2016). Macrophage-secreted granulin supports pancreatic cancer metastasis by inducing liver fibrosis. Nat. Cell Biol. *18*, 549–560. https://doi.org/10.1038/ncb3340.
26. Lin, H., Hu, P., Zhang, H., Deng, Y., Yang, Z., and Zhang, L. (2022). GATA2-Mediated Transcriptional Activation of Notch3 Promotes Pancreatic Cancer Liver Metastasis. Mol. Cell. *45*, 329–342. https://doi.org/10.14348/molcells.2022.2176.
27. Marimuthu, S., Lakshmanan, I., Muniyan, S., Gautam, S.K., Nimmakayala, R.K., Rauth, S., Atri, P., Shah, A., Bhyravbhatla, N., Mallya, K., et al. (2022). MUC16 Promotes Liver Metastasis of Pancreatic Ductal Adenocarcinoma by Upregulating NRP2-Associated Cell Adhesion. Mol. Cancer Res. *20*, 1208–1221. https://doi.org/10.1158/1541-7786.MCR-21-0888.

STAR★METHODS

KEY RESOURCES TABLE

REAGENT or RESOURCE	SOURCE	IDENTIFIER
Antibodies		
RRM2	proteintech	11661-1-AP; RRID:AB_2180392
GAPDH	Abcam	ab8245; RRID:AB_2107448
MIB1	proteintech	11893-1-AP; RRID:AB_2877803
YBX1	proteintech	20339-1-AP; RRID:AB_10665424
TGFBR1	ABclonal	A0708; RRID:AB_2757355
TGFBR2	proteintech	27212-1-AP; RRID:AB_2918119
MDM2	proteintech	27883-1-AP; RRID:AB_2881003
RBBP6	proteintech	11882-1-AP; RRID:AB_2177794
FBXO3	proteintech	17803-1-AP; RRID:AB_2278445
PRPF19	proteintech	15414-1-AP; RRID:AB_10637855
Bacterial and virus strains		
Lentivirus	sigma	N/A
Biological samples		
Tissue microarray	Bioaitech	D049Pa01
Chemicals, peptides, and recombinant proteins		
Dulbecco's modified Eagle medium (DMEM)	Invitrogen	N/A
Fetal bovine serum (FBS)	HyClone	N/A
Lipofectamine 2000	Thermo Fisher Scientific	N/A
proteasome inhibitor MG-132	Selleck	S2619
cycloheximide (CHX)	Selleck	S7418
Trizol reagent	Thermo Fisher Scientific	N/A
Bio-Coat Matrigel	BD Biosciences	N/A
Critical commercial assays		
mycoplasma contamination test kit	Servicebio	G1901-20T
PrimeScript™ RT reagent Kit	Takara	N/A
TB Green™ Fast qPCR Mix	Takara	N/A
Chromatin Extraction Kit	Abcam	ab117152
ChIP Kit Magnetic - One Step	Abcam	ab156907
MTS kit	Abcam	ab197010
Deposited data		
RNA-seq	This paper	GSE274806
Experimental models: Cell lines		
MIA PaCa-2	Chinese Academy of Sciences	N/A
AsPC-1	Chinese Academy of Sciences	N/A
SW1900	Chinese Academy of Sciences	N/A
BxPC-3	Chinese Academy of Sciences	N/A
PANC-1	Chinese Academy of Sciences	N/A
HPDE6-C7	Chinese Academy of Sciences	N/A

(*Continued on next page*)

Continued

REAGENT or RESOURCE	SOURCE	IDENTIFIER
Experimental models: Organisms/strains		
Mouse: BALB/c nude	Shubeili (China)	N/A
Oligonucleotides		
Primers, See Tables S2 and S3	This paper	N/A
Software and algorithms		
R version 4.2.3	R Development Core Team	https://www.r-project.org
GraphPad Prism version 9.0	GraphPad Software	https://www.graphpad.com

EXPERIMENTAL MODEL AND STUDY PARTICIPANT DETAILS

Cell lines

Pancreatic cancer cell lines (SW1990, AsPC-1, MIA PaCa-2, PANC-1 and BxPC-3) and pancreatic ductal epithelial cell line (HPDE6-C7) were obtained from the Chinese Academy of Science Cell Bank. All cell lines were cultured in Dulbecco's modified Eagle medium (DMEM) (Invitrogen, USA) supplemented with 10% fetal bovine serum (FBS) (HyClone, USA). All cell lines were tested for mycoplasma contamination (Servicebio, G1901-20T). PANC-1 and BxPC-3 cells were authenticated as detailed in the supplementary materials (Supplement Materials PANC-1 STR and BxPC-3 STR).

Animal studies

The study was conducted in accordance with the principles of the Declaration of Helsinki principles. It was approved by the Animal Use and Care Committees at Tongji Medical College, Huazhong University of Science and Technology.

([2022] Approval IACUC Number:3643). BALB/c-nude mice aged between 4 and 5 weeks and weighing 18 to 20g were procured from Shubeili (China). Standard living conditions were maintained for the mice, including a 12-h light/dark cycle, free access to food and water.

METHOD DETAILS

Cell transfection

The cells were maintained in a 37°C incubator with 5% CO2. PANC-1 and BxPC-3 cells were seeded into 6-well plates at a density of 2.5×10^5 cells per well and incubated for 24 h before transfection. Transfection was performed using Lipofectamine 2000 (Thermo Fisher Scientific). The multiplicity of infection (MOI) for PANC-1 and BxPC-3 cell lines was established at 10 and 20, respectively, with a viral exposure duration of 6–8 h.

The lentivirus-based control and gene-specific shRNAs (shMIB1#1, shMIB1#2, shRRM2#1, shRRM2#2, shYBX1#1, shYBX1#2, shRBBP6, shPRPF19, shFBXO3, and shMDM2, Sigma-Aldrich) were employed to interfere the expression of gene in 293T cells. Following transfection for 24 h, the transfection medium was replaced with DMEM, which had been prepared with 10% FBS and 1mM sodium pyruvate. Then, the culture solution containing lentivirus was collected after 48 h of continuous culture and provided to PANC-1 and BxPC-3 cells lines supplemented with 12 μg/mL of polybrene. Cells were cultured in 10 μg/mL of puromycin for 24 h to select for successfully infected cells. The specific sequence information of the shRNAs is provided in Table S1.

Co-immunoprecipitation and immunoblotting

Cells were collected and lysed with RIPA lysis buffer (G2002-100ML, Servicebio, China) containing 1% protease and phosphatase inhibitors for 15 min on ice. Using protein assay kit (Pierce Biotechnology, USA) to determine the protein concentrations. Equal quantity of proteins were separated on SDS-PAGE gels and transferred to PVDF membranes, on which specific proteins were detected following sequential incubation with primary and secondary antibodies.

For co-immunoprecipitation, cells were harvested and incubated in 1 mL of IP lysis buffer (G2038-100ML, Servicebio, China) for 20 min on ice. After centrifugation at 15 000 g for 15 min at 4°C, the resulting supernatant was collected and incubated overnight with primary antibody or IgG using Pierce Protein G Agarose (Thermo Fisher Scientific) at 4°C. The beads were then washed five times with IP lysis buffer and resuspended in loading buffer. Subsequently, the beads were boiled at 100°C for 5 min. Immunoblotting analysis was then conducted to analyze the proteins in the pull-down.

RT-qPCR and ChIP-qPCR

Trizol reagent (Thermo Fisher Scientific, USA) was used to extract total RNA from PANC-1 and BxPC-3 cells. Reverse transcription was then performed to prepare cDNA using the PrimeScript RT reagent Kit. Finally, RT-PCR analysis was carried out to amplify and measure the cDNA using a qPCR kit (TB Green Fast qPCR Mix). All Cq values were normalized to GAPDH, and the $2^{-\Delta Cq}$ method was used to describe fold changes.

A Chromatin Extraction Kit (Abcam, ab117152, USA) and ChIP Kit Magnetic - One Step (Abcam, ab156907, USA) were used to perform ChIP. The antibodies used were YBX1 (20339-1-AP; proteintech; 1:100 dilution) and TGFBR1 (A0708; ABclonal; 1:200 dilution). The primer sequences are provided in Table S2 and S3.

In vitro cell growth assay

1×10^4 Pancreatic cancer cells were planted in 96-well plates, and MTS solution (cat. no. ab197010; Abcam) was introduced following the instructions. Absorbance at 490 nm was measured to evaluate *in vitro* cell growth. For the process of colony creation evaluation, the cells were placed in 6-wells plates (500 cells/well) and incubated in a complete growth medium that contained 10% fetal bovine serum (FBS) at a temperature of 37°C.After the course of 14 days, the cells underwent fixation in methanol for a duration of 30 min followed by staining using a 1% solution of Crystal Violet Staining Solution for another 30 min. Subsequently, the plates were rinsed with PBS three times. Finally, the calculation of the total number of colonies was performed.

In vitro invasion assay

The study employed Bio-Coat Matrigel (BD Biosciences, China) invasion chambers for *in vitro* cell invasion assays. Initially, cells were cultivated in the chamber inserts for 24 h and subsequently fixed using methanol for 15 min. Staining with crystal violet for 30 min was done to visualize the cells. The count of invading cells was conducted in a minimum of three fields per group.

In vivo tumor growth assay and liver metastasis assay

To generate xenografts, PANC-1 cells were infected with lentiviral particles of varying types. Following puromycin selection for 48 h, 1×10^7 cells were subcutaneously injected into the mice's back. Measurements of xenografts' length and width were taken using a Vernier caliper, and tumor volumes were calculated using the formula $(L \times W^2)/2$. At the termination of the study, euthanasia was performed on the mice, and the tumors were excised and weighed.

For liver metastasis models, living conditions and anesthesia for mice adhere to the previously described conditions. A minimally invasive incision was made in the abdominal wall to facilitate exposure of the spleen. Subsequently, 1×10^6 PANC-1 cells were inoculated into the spleen, following the identical cell preparation and murine procedures outlined earlier. Thirty minutes post-inoculation, the spleen was excised, and hemostasis was secured utilizing an electrocautery device. The abdominal incision was then meticulously closed, and the surgical site was disinfected. After 4 weeks, the mice were euthanized and livers were harvested for paraffin embedding and HE staining.

Tissue microarray and immunohistochemistry (IHC)

Tissue microarray (D049Pa01, Bioaitech, China) and IHC were employed to assess the levels of RRM2 (11661-1-AP; proteintech; 1:400 dilution), YBX1 (20339-1-AP; proteintech; 1:2000 dilution) and TGFBR1 (A0708; ABclonal; 1:900 dilution) in pancreatic cancer. The evaluation of the IHC score depended on both the staining intensity and the proportion of positive tumor cells. The scoring of staining intensity was as follows: 1 = weak staining at 100× magnification and limited or absent staining at 40× magnification; 2 = moderate staining at 40× magnification; 3 = strong staining at 40× magnification. Two experienced pathologists, who were unaware of the study, independently determined the IHC scores.

The cells were maintained in a 37°C incubator with 5% CO2. PANC-1 and BxPC-3 cells were seeded into 6-well plates at a density.

Immunofluorescence co-localization

2×10^5 PANC-1 and BxPC-3 cells were seeded onto glass slides within 6-well plates and cultured at 37°C in an incubator with 5% CO2 for an overnight period. The cells were subsequently fixed with 1 mL of a 4% paraformaldehyde solution for 30 min, followed by rinsing with phosphate-buffered saline (PBS) in triplicate for 3 min each. Permeabilization was performed using 0.5% Triton X-100 (Servicebio, China, G1204-100ML) for 30 min, after which the cells were again rinsed with PBS in triplicate for 3 min each. Cells were then treated with 1% bovine serum albumin (BSA) for 30 min to block non-specific binding, after which the blocking solution was aspirated. Primary antibodies specific for YBX1 (20339-1-AP; Proteintech, diluted 1:500) and RRM2 (67006-1 Ig; Proteintech, diluted 1:100) were incubated with the cells at 4°C overnight. Following three rinses with PBS for 3 min each, the cells were incubated with CoraLite488-conjugated Goat Anti-Rabbit IgG (SA00013-2; Proteintech, diluted 1:100) and Multi-rAb CoraLite Plus 594-Goat-Anti-Mouse Recombinant Secondary Antibody (RGAM0004; Proteintech, diluted 1:200) for 1 h. After three additional rinses with PBS for 3 min each, the nuclei were counterstained with DAPI for 5 min. Finally, the cells were rinsed three times for 5 min each with PBS, and the glass slides with adherent cells were mounted using an anti-fluorescence quenching medium (Servicebio, China, G1401-5ML). The slides were allowed to dry before being visualized under confocal microscopy.

Bioinformatics analysis

Bioinformatics analysis in this study are sourced from the following databases: The Cancer Genome Atlas (TCGA), Gene Expression Omnibus (GEO), CancerSEA, and ChIP-Atlas (Details in Supplementary Methods).

(1) TCGA-PAAD: Transcriptome data and clinical information of LUAD patients were obtained from the GDC data portal (https://portal.gdc.cancer.gov/).

(2) EXP0060: Transcriptome data of single cells from BCH869 PDX model were obtained from the CancerSEA database (http://biocc.hrbmu.edu.cn/CancerSEA/).
(3) EXP0066: Transcriptome data of single cells from LC-PT-45 cell line were obtained from the CancerSEA database (http://biocc.hrbmu.edu.cn/CancerSEA/).
(4) GSE117924: Transcriptome data of human prostate cancer C4-2 cells transfected with siRNAs (siNS and siRRM2) were obtained from the GEO database (https://www.ncbi.nlm.nih.gov/).
(5) Survival analysis: Patients were divided into two groups according to the median expression level of the key gene. The differences in RFS/No Liver Metastasis RFS/OS between the high and low expression groups were evaluated by the Kaplan–Meier method, followed by a log rank test.
(6) ChIP-Atalas: Binding site in the targeted gene promoter of the key protein were obtained from ChIP-Atlas database (https://chip-atlas.org/).
(7) CUCKOO: Predicting the possible ubiquitination E3 of YBX1 by PTMs Predictors (GPS-Uber) (http://www.biocuckoo.org).
(8) Ubibrowser: Predicting the possible ubiquitination E3 of YBX1 by Ubibrowser 2.0 (http://ubibrowser.bio-it.cn/ubibrowser_v3/).

QUANTIFICATION AND STATISTICAL ANALYSIS

Statistical analysis in this study were conducted using the GraphPad Prism 9 software. Descriptive statistics are presented as means ± standard deviation (SD). The sample size (*n* values) for each analysis can be found in the figure captions. Statistical significance was assessed using Student's t-test for comparisons between two groups and one-way or two-way ANOVA for comparisons among multiple groups. Results with a *p*-value less than 0.05 were deemed statistically significant. Microsoft R Open v4.0.2 was used for data mining, bioinformatics analysis and visualization in transcriptomics and proteomics data. IGV v2.9.0 was used for analysis and visualization of ChIP-seq data.